Fe L-Edge XAS Studies of K$_4$[Fe(CN)$_6$] and K$_3$[Fe(CN)$_6$]: A Direct Probe of Back-Bonding

Rosalie K. Hocking,[†] Erik C. Wasinger,[†] Frank M. F. de Groot,*,[‡]
Keith O. Hodgson,*,[†,§] Britt Hedman,*,[§] and Edward I. Solomon*,[†]

*Contribution from the Department of Chemistry, Stanford University,
Stanford, California 94305, Department of Inorganic Chemistry and Catalysis, Utrecht
University, Sorbonnelaan 16, 3584 Utrecht, The Netherlands, and Stanford Synchrotron
Radiation Laboratory, SLAC, Stanford University, Stanford, California 94309*

Received March 15, 2006; E-mail: f.m.f.degroot@chem.uu.nl; hodgson@ssrl.slac.stanford.edu;
hedman@ssrl.slac.stanford.edu; edward.solomon@stanford.edu

Abstract: Distinct spectral features at the Fe L-edge of the two compounds K$_3$[Fe(CN)$_6$] and K$_4$[Fe(CN)$_6$] have been identified and characterized as arising from contributions of the ligand π^* orbitals due to metal-to-ligand back-bonding. In addition, the L-edge energy shifts and total intensities allow changes in the ligand field and effective nuclear charge to be determined. It is found that the ligand field term dominates the edge energy shift. The results of the experimental analysis were compared to BP86 DFT calculations. The overall agreement between the calculations and experiment is good; however, a larger difference in the amount of π back-donation between Fe(II) and Fe(III) is found experimentally. The analysis of L-edge spectral shape, energy shift, and total intensity demonstrates that Fe L-edge X-ray absorption spectroscopy provides a direct probe of metal-to-ligand back-bonding.

Introduction

The chemical bonding between a transition metal and a ligand such as CN$^-$ or CO is generally described in terms of donor interactions between occupied orbitals of the ligand and the unoccupied and partially occupied orbitals of the metal, and acceptor interactions between the occupied or partly occupied orbitals of the metal and the unoccupied orbitals of the ligand. The model most widely invoked to describe such bonding interactions is that of Dewar, Chatt, and Duncanson,[1–3] in which σ donation and π acceptance are described as having a synergistic bonding effect (Figure 1). Homoleptic octahedral complexes of transition metals have played a fundamental role in developing many ideas in coordination chemistry because their molecular orbital and bonding picture is simplified by symmetry.[4–6] Among the most widely investigated systems that display back-bonding are the iron(II) and iron(III) hexacyanides.[7–12]
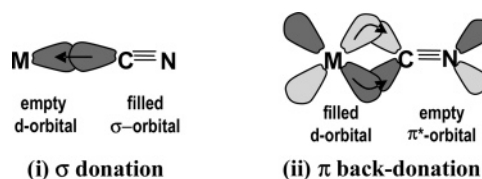

Figure 1. Schematic illustration of the Dewar−Chatt−Duncanson model for back-bonding.

(i) σ donation — empty d-orbital, filled σ−orbital

(ii) π back-donation — filled d-orbital, empty π*-orbital

The absorption spectra of [Fe(CN)$_6$]$^{3-}$ and [Fe(CN)$_6$]$^{4-}$ were originally reported as early as the 1940s.[13–18] The 10Dq values of these compounds are large compared with those of σ-only donor complexes, and there is little difference between the 10Dq values observed for [Fe(CN)$_6$]$^{4-}$ and [Fe(CN)$_6$]$^{3-}$.[13–18] In addition to the ligand field (d−d) transitions, intense absorption bands were observed which were assigned as arising from metal-to-ligand charge-transfer transitions, providing further evidence for π back-bonding.[16] Around the same time as the absorption spectra were investigated, substantial research focused on the force constants of metal−carbon and carbon−nitrogen bonds.[19–22] These were also interpreted in terms of σ donation and π back-

† Department of Chemistry, Stanford University.
‡ Utrecht University.
§ Stanford Synchrotron Radiation Laboratory.
(1) Dewar, M. J. S. *Bull. Soc. Chim. Fr.* **1951**, *18*, C71−C79.
(2) Frenking, G. *J. Organomet. Chem.* **2001**, *635*, 9−23.
(3) Chatt, J.; Duncanson, L. A. *J. Chem. Soc.* **1953**, 2939−2947.
(4) Lever, A. B. P.; Solomon, E. I. In *Inorganic Electronic Structure and Spectroscopy*; Solomon, E. I., Lever, A. B. P., Eds.; Wiley: New York, 1999; Vol. 1, pp 1−91.
(5) Gray, H. B.; Ballhausen, C. J. *J. Am. Chem. Soc.* **1963**, *85*, 260−265.
(6) Ballhausen, C. J.; Gray, H. B. *Molecular Orbital Theory*; W. A. Benjamin Inc.: New York, 1964.
(7) Smith, S.; Taylor, D. A.; Hillier, I. H.; Vincent, M. A.; Guest, M. F.; MacDowell, A. A.; von Niessen, W.; Urch, D. S. *J. Chem. Soc., Faraday Trans.* **1988**, *84*, 209−217.
(8) Figgis, B. N.; Kucharski, E. S.; Raynes, J. M.; Reynolds, P. A. *J. Chem. Soc., Dalton Trans.* **1990**, 3597−3604.
(9) Brown, P. J.; Day, P.; Fischer, P.; Guedel, H. U.; Herren, F.; Ludi, A. *J. Phys. Coll.* **1982**, *C-7*, 235−240.

(10) Fletcher, S. R.; Gibb, T. C. *J. Chem. Soc., Dalton Trans.* **1977**, 309−317.
(11) Bergknut, L.; Andermann, G.; Haycock, D.; Kasrai, M.; Urch, D. S. *J. Chem. Soc., Faraday Trans.* **1981**, *77*, 1879−1889.
(12) Calabrese, A.; Hayes, R. G. *J. Am. Chem. Soc.* **1974**, *96*, 5054−5062.
(13) Kiss, A. V.; Abraham, J.; Hegedus, I. *Z. Anorg. Allg. Chem.* **1940**, *244*, 98−100.
(14) Parsons, R. W.; Drickamer, H. G. *J. Chem. Phys.* **1958**, *29*, 930−937.
(15) Naiman, C. S. *J. Chem. Phys.* **1961**, *35*, 323−328.
(16) Alexander, J. J.; Gray, H. B. *J. Am. Chem. Soc.* **1968**, *90*, 4260−4271.
(17) Alexander, J. J.; Gray, H. B. *Coord. Chem. Rev.* **1967**, *2*, 29−43.
(18) Naiman, C. S. *J. Chem. Phys.* **1962**, *35*, 323−333.
(19) Ginsberg, A. P.; Koubrek, E. *Inorg. Chem.* **1965**, *4*, 1186−1194.
(20) Jones, L. H. *J. Chem. Phys.* **1962**, *36*, 1209−1212.
(21) Jones, L. H. *J. Chem. Phys.* **1964**, *41*, 856−863.
(22) Mathieu, J. P.; Poulet, H. *Spectrochim. Acta* **1963**, *19*, 1966.

donation.[23] It was first understood experimentally,[21] and later shown with molecular orbital (MO) calculations, that both the $5\sigma^+$ occupied and $2\pi^*$ unoccupied orbitals are antibonding with respect to the CN^- bond.[24,25] This means that σ donation has the effect of shortening the $C-N$ distance, whereas π back-donation lengthens it. From this relationship, periodic trends in the bonding to transition metals could be observed based on vibrational frequencies.[23,26] It was found that $[Fe(CN)_6]^{4-}$ has a lower CN^- force constant than $[Fe(CN)_6]^{3-}$. This had been interpreted as an increase in back-donation in $[Fe(CN)_6]^{4-}$ over $[Fe(CN)_6]^{3-}$.[26] However, these analyses are complicated by two factors. First, the CN^- vibrations can be affected by mechanical coupling to the $Fe-C$ stretch, shifting the interligand vibration to higher energy. Second, while σ donation and π back-donation have opposite effects on the $C-N$ bond strength, their relative magnitudes cannot be uncoupled from the net vibrational frequency. So, as with absorption data, evidence for back-bonding is found from vibrational spectroscopy, but it does not quantify the relative contributions of σ donation and π back-donation.[7−12] Further, these techniques do not directly allow a comparison of the contributions of π back-bonding between two compounds with different ligand sets.

Molecular orbital calculations complement experiments. Good examples for the determination of the relative contributions of σ donation and π back-donation in terms of both molecular orbital coefficients and energetics are given in refs 16, 17, 27−31. Several studies of $[Fe(CN)_6]^{3-}$ and $[Fe(CN)_6]^{4-}$ have been performed using different computational techniques and population analyses.[7,30,32−34] When studies with the same functional/basis set are compared, it is consistently found that π back-bonding from Fe is slightly greater in $[Fe(CN)_6]^{4-}$ than in $[Fe(CN)_6]^{3-}$. However, the characterization of the degree of σ donation relative to π back-bonding varies substantially, depending on the technique used.[17,27,28,30,33]

Fe L-edge X-ray absorption spectroscopy (XAS) provides a number of key probes of bonding. The $2p \rightarrow 3d$ transition is electric dipole allowed, which means that the Fe L-edge intensity is directly proportional to the Fe d-character in the unoccupied orbitals of the metal. In previous studies, where systems contain only ligand-to-metal donation, this meant that total intensity was proportional to covalency.[35−38] The shape of the spectrum permits insight into the ligand field but is convoluted by multiplet contributions similar to the effects described by the

Tanabe−Sugano[39] diagrams for d^N metal complexes but for the $2p^5 3d^{N+1}$ final states. A further contribution to the L-edge shape is the effect of covalency. In the ground state, the d^N configuration mixes with the $d^{N+1}\underline{L}$ configuration by ligand−donor bonding (a ligand-to-metal charge-transfer, LMCT, process) and with the $d^{N-1}L^-$ configuration by ligand−acceptor bonding (metal-to-ligand charge-transfer, MLCT, process), where L^- is an extra ligand electron and $\underline{L}$ is a ligand hole. This mixing can cause changes to the L-edge spectral shape, including the appearance of satellite structure on the high-energy side of the L_3/L_2 edges. Note that the 2p hole spin−orbit couples to give the $J = {}^3/_2$ (L_3) and $J = {}^1/_2$ (L_2) edges split by ∼20 eV.

As mentioned above, the shapes of the L-edges of the 3d transition metal series have contributions from two factors: multiplet effects and ligand field splittings. The effects of these can be calculated using the ligand field multiplet model implemented by Thole.[40] In early analysis, the effect of covalency on the L-edge was accounted for only by the reduction of the Slater integrals associated with electron repulsion (by $\kappa < 1$).[41−43] Later versions of the model included the charge-transfer effects of covalency by explicitly allowing each symmetry set of metal d orbitals and ligand configurations to mix using a valence bond configuration interaction (VBCI) model. Both the LMCT model and the crystal field model have been applied to model Fe L-edge spectral shape.[44,45] Arrio and co-workers have analyzed a number of cubic systems with CN^- ligands bridging two transition metal sites.[41−43,46] It was found for the Cr sites of these compounds that the LMCT model could not reproduce the shape of the spectra, and the multiplet model was adapted to include the effects of MLCT, which successfully reproduced the spectral shapes.

Recently, a methodology has been developed,[38] based on multiplet simulations, that enables the determination of the covalent delocalization of the different symmetry sets of d orbitals, called differential orbital covalency (DOC). For $[Fe(tacn)_2]^{2+/3+}$, a σ-only donor-based amine ligand system, this enabled the determination of the covalency of the e_g and t_{2g} sets, showing that the t_{2g} covalency was negligibly small. Thus far, the technique has been applied only to systems where ligand-to-metal donation is present. Herein the multiplet structures of the Fe L-edges of $K_4[Fe(CN)_6]$ and $K_3[Fe(CN)_6]$ are analyzed in terms of total intensity, energy shift, and spectral shape. The TT-multiplet program is adapted to simultaneously include MLCT and LMCT, enabling us to use the Fe L-edge multiplet structure combined with DOC to experimentally quantify the σ- and π-donor, and in particular the contributions of π back-bonding to Fe−cyanide bonding. Importantly, there is an additional intense feature to higher energy of the main peak in the L-edge spectrum of compounds with significant back-

(23) Jones, L. H. *Inorg. Chem.* **1963**, *2*, 777−780.
(24) Fenske, R. F.; deKock, R. L.; Sarapu, A. C. *Inorg. Chem.* **1971**, *10*, 38−43.
(25) Polak, R.; Fiser, J. *Theochem* **2002**, *584*, 69−77.
(26) Jones, L.; Swanson, B. I. *Acc. Chem. Res.* **1976**, *9*, 128−134.
(27) Loschen, C.; Frenking, G. *Inorg. Chem.* **2004**, *43*, 778−784.
(28) Frenking, G.; Wichmann, K.; Frohlich, N.; Loschen, C.; Lein, M.; Frunzke, J.; Rayon, V. M. *Coord. Chem. Rev.* **2003**, *238−239*, 55−82.
(29) Hummel, P.; Oxgaard, J.; Goddard, W. A.; Gray, H. B. *J. Coord. Chem.* **2005**, *58*, 41−45.
(30) Sano, M.; Adachi, H.; Yamatera, H. *Bull. Chem. Soc. Jpn.* **1981**, *54*, 2898−2903.
(31) Pierloot, K.; Van Praet, E. V.; Vanquickenborne, L. G.; Roos, B. O. *J. Phys. Chem.* **1993**, *97*, 12220−12228.
(32) Fenske, R. F.; DeKock, R. L. *Inorg. Chem.* **1972**, *11*, 437−444.
(33) Sano, M.; Kashiwagi, H.; Yamatera, H. *Inorg. Chem.* **1982**, *21*, 3837−3841.
(34) Larsson, S. *Theor. Chim. Acta* **1978**, *49*, 45−53.
(35) George, S. J.; Lowery, M. D.; Solomon, E. I.; Cramer, S. P. *J. Am. Chem. Soc.* **1993**, *115*, 2968−2969.
(36) Kotani, A.; Okada, K. *Tech. Rep. ISSP, Ser. A* **1992**, 2562.
(37) van der Laan, G.; Zaanen, J.; Sawatzky, G. A.; Karnatak, R.; Esteva, J. M. *Phys. Rev. B* **1986**, *33*, 4253−4263.
(38) Wasinger, E. C.; deGroot, F. M. F.; Hedman, B.; Hodgson, K. O.; Solomon, E. I. *J. Am. Chem. Soc.* **2003**, *125*, 12894−12906.

(39) Sugano, S.; Tanabe, Y. *Multiplets of transition-metal ions in crystals*; Academic Press: New York, 1970.
(40) Thole, B. T.; van der Laan, G.; Fuggle, J. C.; Sawatzky, G. A.; Karanatak, R. C.; Esteva, J.-M. *Phys. Rev. B* **1985**, *32*, 5107−5118.
(41) Arrio, M.-A.; Sianctavit, Ph.; Cartier dit Moulin, Ch.; Mallah, T.; Verdaguer, M.; Pellegrin, E.; Chen, C. T. *J. Am. Chem. Soc.* **1996**, *118*, 6422−6427.
(42) Arrio, M.-A.; Sciuller, A.; Sainctavit, Ph.; Cartier dit Moulin, Ch.; Mallah, T.; Verdaguer, M. *J. Am. Chem. Soc.* **1999**, *121*, 6414−6420.
(43) Cartier dit Moulin, Ch.; Villain, F.; Bleuzen, A.; Arrio, M. A.; Sainctavit, C.; Lomenech, C.; Escax, V.; Baudelet, F.; Dartyge, E.; Gallet, J. J.; Verdaguer, M. *J. Am. Chem. Soc.* **2000**, *122*, 6653−6658.
(44) Wang, H.; Peng, G.; Miller, L. M.; Scheuring, E. M.; George, S. J.; Chance, M. R.; Cramer, S. P. *J. Am. Chem. Soc.* **1997**, *119*, 4921−4928.
(45) deGroot, F. M. F. *Coord. Chem. Rev.* **2005**, *249*, 31−63.
(46) Briois, V.; Cartier dit Moulin, Ch.; Sainctavit, P.; Brouder, Ch.; Flank, A.-M. *J. Am. Chem. Soc.* **1995**, *117*, 1019−1026.

bonding. The nature of this feature and the origin of its high intensity are determined. These studies demonstrate the power of metal L-edge XAS to recognize and quantify π back-bonding in transition metal compounds.

Experimental Section

Samples. $K_4[Fe(CN)_6]$ and $K_3[Fe(CN)_6]$ were purchased from Sigma Aldrich and used without further purification. Samples were finely ground and spread across double-sided adhesive conductive graphite tape and attached to a copper paddle, aligned 45° to the incident beam as described previously.[38,47]

XAS Data Collection. X-ray absorption spectra were recorded at the Stanford Synchrotron Radiation Laboratory (SSRL) on the 31-pole wiggler beam line 10-1 under ring operating conditions of 50−100 mA and 3 GeV. The radiation was monochromatized using a spherical grating monochromator set at 1000 lines/mm and 20 μm entrance and exit slits. All measurements were made at 20 ± 5 °C. The energy was calibrated from the Fe L-edge spectra of Fe_2O_3, run at intervals between scans. The second feature in the L_3 edge and the first feature in the L_2 edge were calibrated to 708.5 and 720.1 eV, respectively. Data were taken over the range 670−830 eV to permit normalization as described previously.[38] A step size of 0.1 eV was used over the edge region (700−730 eV) and 0.5 eV steps over the remaining regions. A function of the form absorption = $[\tan^{-1}(k(\text{energy} - I_1) + \pi/2)(2/3)(1/\pi)]$ $+[\tan^{-1}(k(\text{energy} - I_2) + \pi/2)(1/3)(1/\pi)]$, where $k = 0.295$ (obtained by experimental fit)[38,48] and $I_2 = I_1 + 12.3$ eV (due to spin−orbit coupling), was used to model the L_3- and L_2-edge jumps, as described previously.[38] For the $K_4[Fe(CN)_6]$/$K_3[Fe(CN)_6]$ data, the absolute energy of the arctangent was estimated on the basis of a combination of photoelectron spectroscopy (PES) data and a fit to the L-edge spectra.[7,11,38] The post-normalization L_3 intensities reported here were calculated as the intensity in the range 700−715 eV for $[Fe(tacn)_2]Cl_2$, 703−718 eV for $K_4[Fe(CN)_6]$, 701−716 eV for $[Fe(tacn)_3]Cl_3$, and 702.5−717.5 eV for $K_3[Fe(CN)_6]$, and the L_2 intensities for the normalized ranges were 715−730 eV for $[Fe(tacn)_2]Cl_2$, 718−733 eV for $K_4[Fe(CN)_6]$, 716−731 eV for $[Fe(tacn)_2]Cl_3$, and 717.5−732.5 eV for $K_3[Fe(CN)_6]$. The different energy ranges were used to account for differences in spectral shift. The error reported represents the range of integrated intensities calculated as defined above, based on at least three repeat measurements of the same spectra on different dates. Numbers reported have the units of Abs·eV or normalized intensity.

Computational Details

Multiplet Calculations. Ligand field multiplet calculations were performed using the multiplet model implemented by Thole,[40] the atomic theory developed by Cowan,[49] and the crystal field (i.e., symmetry) interactions described by Butler.[50] This approach includes both electronic Coulomb interactions and spin−orbit coupling for each sub-shell.[41,51] To simulate the spectra, the Slater−Condon−Shortley parameters (F_i and G_i) were first reduced to 80% of their Hartree− Fock calculated values to account for the over-estimation of electron− electron repulsion found in calculations of the free ion. The spectrum is calculated from the sum of all possible transitions for an electron excited from the 2p level into a 3d level.[52] To model ligand-to-metal and metal-to-ligand charge transfer (LMCT and MLCT), the ground state of a $3d^N$ ion is taken to be a linear combination of three

configurations, $3d^{N-1}$ $\underline{L}^-$, $3d^N$, and $3d^{N+1}$ $\underline{L}$. To compare to experiment, calculated transitions were Lorentzian broadened with a fwhm of 0.2 eV over the L_3 edge and 0.4 eV over the L_2 edge to allow for lifetime broadening, and with a Gaussian fwhm of 0.2 eV to allow for instrumental broadening effects as described elsewhere.[53] Further technical details and program input files for implementation of the three configuration simulations, including both LMCT and MLCT in the multiplet program, are given in the Supporting Information.

The effects of the different contributions to bonding were considered systematically. First, the effects of back-bonding were considered by MLCT simulations, then the addition of σ donation and other effects such as π donation and σ back-donation were considered. Parameters that determined the energy separation (Δ) between the d^N, d^{N-1} $\underline{L}^-$, and d^{N+1} $\underline{L}$ configurations, EG2(d^{N-1} and d^N); EG3(d^{N-1} and d^{N+1}) (ground state) and EF2(d^{N-1} and d^N); EF3(d^{N-1} and d^{N+1}) (final state), and the values of T_i, the parameters which allow for the covalent overlap of different symmetry components (i), were chosen on the basis of previous results and then systematically varied to optimize the spectral fit.[54]

DFT Calculations. The starting structures of the two compounds $[Fe(CN)_6]^{4-}$ and $[Fe(CN)_6]^{3-}$ were idealized in O_h symmetry to the average of all structures of these ions obtained by a search of the Cambridge Structural Database.[55] DFT calculations were performed using ADF.[56−58] The geometries were optimized using the exchange functional of Becke[59] and the correlation functional of Perdew (BP86).[60] The frozen core approximation[61] was used for the 1s−2p orbitals for iron. For valence orbitals, Slater-type orbital (STO) basis sets of triple-ζ quality were employed with polarization function on the ligand atoms (3d) and additional valence p orbitals on the metal atoms (i.e., ADF basis set IV).[57,58,62] This basis set combination has been shown to give a well-converged solution.[63,64] Population analyses were performed using the Mulliken[56] approach as implemented in ADF. The ADF fragment approach was used to separate σ-donor, π-donor, and π-acceptor contributions to bonding.[57,58,62]

Results

Fe(II) L-Edge. Figure 2a shows the normalized L-edge absorption spectra of $K_4[Fe(CN)_6]$ and $[Fe(tacn)_2]Cl_2$. Two major differences can be seen between the two spectra. The main feature of the $K_4[Fe(CN)_6]$ spectrum shifts 1.4 eV to higher energy (Table 1), and the spectrum changes shape with an additional intense peak to higher energy, relative to the spectrum of $[Fe(tacn)_2]Cl_2$. The total intensities of the two spectra are the same within error, 36(4) units for $K_4[Fe(CN)_6]$ and 37(5) for $[Fe(tacn)_2]Cl_2$ (Table 2). The total intensity at the Fe L-edge reflects the total d character in the unoccupied orbitals.[65] On the basis of calibrated intensities of reference compounds, 80.2% metal character corresponds to 50.5 units of L-edge intensity.[38]

(47) DeBeer George, S.; Metz, M.; Szilagyi, R. K.; Wang, H.; Cramer, S. P.; Lu, Y.; Tolman, W. B.; Hedman, B.; Hodgson, K. O.; Solomon, E. I. *J. Am. Chem. Soc.* **2001**, *123*, 5757−5767.
(48) Yeh, J. J.; Lindau, I. *At. Data Nucl. Data Tables* **1985**, *32*, 1−155.
(49) Cowan R. D. *The Theory of Atomic Structure and Spectra*; University of California Press: Berkeley, 1981.
(50) Butler P. H. *Point Group Symmetry Applications: Methods and Tables*; Plenum Press: New York, 1981.
(51) van der Laan, G.; Kirkman, I. W. *J. Phys.: Condens. Matter* **1992**, *4*, 4189−4204.
(52) Bianconi, A.; Della Longa, S.; Li, C.; Pompa, M.; Congui-Castelllano, A.; Udron, D.; Flank, A.-M.; Lagarde, P. *Phys. Rev. B* **1991**, *44*, 10126−10138.

(53) deGroot, F. M. F.; Fuggle, J. C.; Thole, B. T.; Sawatzky, G. A. *Phys. Rev.* **1990**, *B41*, 928−238.
(54) Online Manual for the TT-Multiplets Program (http://www.anorg.chem.uu.nl/people/staff/FrankdeGroot/ttmultiplets.htm), 2005.
(55) Quest 3D, a program for searching the CSD; CCDC: Cambridge, UK, 1994.
(56) Mulliken, R. S. *J. Chem. Phys.* **1955**, *23*, 1833−1840.
(57) Scientific Computing and Modelling NV. *ADF User's Guide*; SCM: Amsterdam, 1999.
(58) Baerends, E. J.; et al. *ADF Program System*, V.01; Scientific Computing and Modeling: Amsterdam, 2000.
(59) Becke, A. D. *Phys. Rev. A* **1988**, *38*, 3098−3100.
(60) Perdew, J. P. *Phys. Rev. B* **1986**, *33*, 8822−8824.
(61) Baerends, E. J.; Ellis, D. E.; Ros, P. *Theor. Chim. Acta* **1972**, *27*, 339−354.
(62) Te Velde, G.; Baerends, E. J.; Fonseca, G. C.; Van Gisbergen, S. J. A.; Snijders, J. G.; Ziegler, T. *J. Comput. Chem.* **2001**, *22*, 931−967.
(63) Ryde, U.; Olsson, M. H. M.; Pierloot, K. In *Theoretical and Computational Chemistry*; Elsevier: Amsterdam, 2001; Vol. 9, pp 1−55.
(64) Siegbahn, P. E. M.; Blomberg, M. R. A. *Chem. Rev.* **2000**, *100*, 421−437.
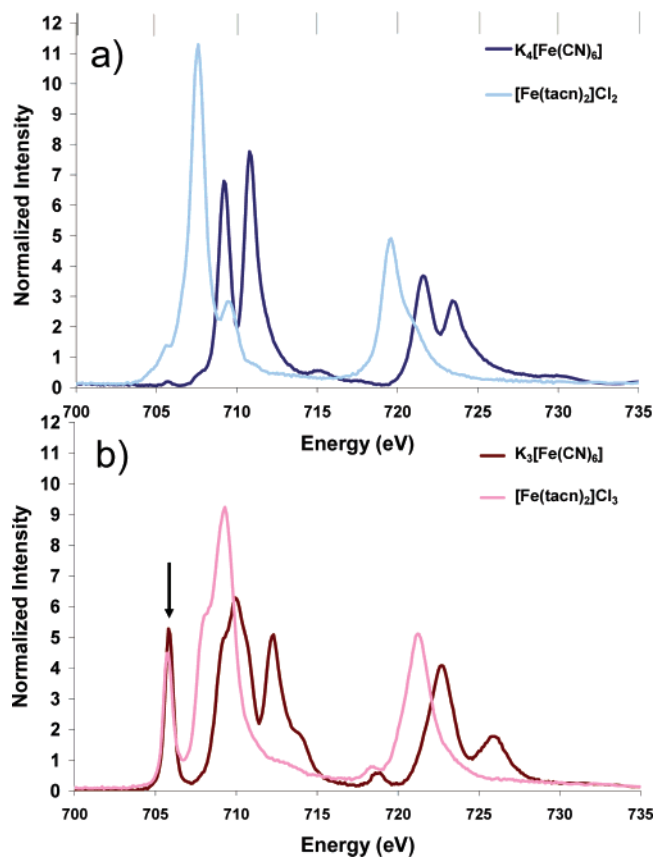(65) Shadle, S. E.; Hedman, B.; Hodgson, K. O.; Solomon, E. I. *Inorg. Chem.* **1994**, *33*, 4235−4255.

Figure 2. Comparison of Fe L-edges of (a) Fe(II) $K_4[Fe(CN)_6]$ and [Fe-$(tacn)_2]Cl_2$ and (b) Fe(III) $K_3[Fe(CN)_6]$ and $[Fe(tacn)_2]Cl_3$. Arrow indicates the feature arising from the $2p^6 t_{2g}^5 \rightarrow 2p^5 t_{2g}^6$ transition (t_{2g} peak) characteristic of low-spin Fe(III) spectra.

Table 1. Maximum Transition Energy (eV) of the L_3 and L_2 Edges of $K_4[Fe(CN)_6]$, $K_3[Fe(CN)_6]$, $[Fe(tacn)_2]Cl_2$, and $[Fe(tacn)_2]Cl_3$

compound	L_3 intensity (energy)	L_2 intensity (energy)	branching ratio $L_3/(L_2 + L_3)$	branching ratio (t_{2g} feature)
$K_4[Fe(CN)_6]$	20.9 (709.2)	15.07 (721.6)	0.58	N/A
$[Fe(tacn)_2]Cl_2$	23.76 (707.8)	12.77 (720.1)	0.65	N/A
$K_3[Fe(CN)_6]$	28.40 (709.9)	14.52 (722.5)	0.66	0.90
$[Fe(tacn)_2]Cl_3$	27.46(709.3)	13.54(721.3)	0.67	0.89

Applying this calibration, the sum of the metal d character in unoccupied orbitals of $K_4[Fe(CN)_6]$ is 287(30)% and that for $[Fe(tacn)_2]Cl_2$ is 295(40)%.

Fe(III) L-Edge. Figure 2b shows the normalized spectra of $[Fe(tacn)_2]Cl_3$ and $K_3[Fe(CN)_6]$. The changes on going from a tacn to a cyanide ligand set in Fe(III) are similar to those in Fe(II), in that an additional large, intense peak is present at higher energy. The shift to higher energy of the main feature on going from tacn to cyanide ligation is less in Fe(III) (0.7 eV) than in Fe(II) (1.4 eV) (Table 1). The spectra for the Fe-(III) compounds also display a sharp peak at lower energy, indicated by the arrow in Figure 2, which is not present for the Fe(II) analogues. This feature is due to the transition to the additional t_{2g} hole in the d manifold on going from low-spin Fe(II) (t_{2g}^6) (Figure 2a) to low-spin Fe(III) (t_{2g}^5)[38,66] (Figure 2b). The energy position of this feature relative to the main multiplet packet is affected by both 10Dq and multiplet interactions.[38]

(66) Cartier dit Moulin, Ch.; Rudolf, P.; Flank, A.-M.; Chen, C.-T. *J. Phys. Chem.* **1992**, *96*, 6196−6198.

Finally, as for Fe(II), the total intensity does not change significantly on going from a tacn to a CN^- donor set. For K_3-$[Fe(CN)_6]$, 43(5) units of intensity is observed and for $[Fe(tacn)_2]$-Cl_3 41(5) units is observed, giving a corresponding sum % metal d character in unoccupied orbitals of 334(40)% and 326(40)%, respectively.

Analysis. 1. Contributions to the Energy Position of the Fe L-Edge Transitions. The CN^- spectra shift to higher energy than the tacn spectra (Figure 2), and this difference is larger for Fe(II) (1.4 eV) than for Fe(III) (0.7 eV). The energy positions of K-edges and, to a lesser extent, L-edges are often used as a measure of Z_{eff} (the effective nuclear charge on the metal).[47,67] Thus, the differences could be interpreted as differences in π back-donation relative to σ donation. However, since the L-edge intensity and edge shift are dominated by transitions to the d orbitals, the effects of ligand field on energy shift must be considered in addition to Z_{eff}. Ligand field contributions to the edge energy of the tacn and CN^- compounds can be estimated from absorption data.[68−70] As the L-edge intensity is proportional to the total metal character in the unoccupied orbitals, it provides an independent measure of Z_{eff}.

a. Fe(II). The contributions of Z_{eff} and ligand field to the relative energy shifts of the $K_4[Fe(CN)_6]$ and $[Fe(tacn)_2]Cl_2$ spectra are illustrated in Figure 3a. The total integrated intensities of $[Fe(tacn)_2]Cl_2$ and $K_4[Fe(CN)_6]$ are the same within error (Table 2), indicating that the difference in Z_{eff} between the two compounds is in fact small. This is indicated in Figure 3 by placing the horizontal thick gray line through the weighted average of the d manifold energies. The 10Dq values of $[Fe(CN)_6]^{4-}$ and $[Fe(tacn)_2]^{2+}$ have been reported to be 4.19 eV[15] and 2.35 eV, respectively.[68−70] Differences in 10Dq affect the L-edge energy because transitions occur only to unoccupied d orbitals. For low-spin Fe(II), the L-edge intensity arises from the transitions to the unoccupied e_g set, which are shifted by $(^3/_5)$10Dq to higher energy relative to the average energy of the d manifold (determined by Z_{eff}). On the basis of these 10Dq values, the spectrum of $K_4[Fe(CN)_6]$ should shift to $\sim(4.19 - 2.35)(^3/_5) = 1.1$ eV higher energy relative to that of $[Fe(tacn)_2]$-Cl_2, close to the experimental shift of 1.4 ± 0.1 eV.

b. Fe(III). For low-spin Fe(III) complexes, the contributions to the energy shifts of the L-edge are similar to those of Fe(II), but with an additional contribution due to the t_{2g} hole. The presence of the t_{2g} hole changes the energy weighting to $(^1/_5)$-$(4(^3/_5)10Dq - 1(^2/_5)10Dq)$ (Figure 3b, marked as "**"). On the basis of ligand field differences, the expected shift of $K_3[Fe-(CN)_6]$ would be 0.78 eV to higher energy relative to $[Fe(tacn)_2]$-Cl_2. The total integrated intensity of $K_3[Fe(CN)_6]$ is similar to that for $[Fe(tacn)_2]Cl_3$ (42(5)/41(5), Table 2), indicating that Z_{eff} is similar in both compounds.[47,71] Thus, the observed shift of 0.7 eV is again mostly accounted for by the difference in ligand field.

From the above analysis, it is the total intensity of the L-edge, not the energy shift of the edge, that reflects the Z_{eff} of the metal.

(67) Ghatikar, M. N.; Padalia, B. D. *J. Phys. C: Solid State Phys.* **1978**, *11*, 1941−1955.
(68) Ventor, D.; Wieghardt, K.; Nuber, B.; Weiss, J. Z. *Z. Anorg. Allg. Chem.* **1987**, *551*, 33−60.
(69) Wieghardt, K.; Schmidt, W.; Herrmann, W.; Kuppers, H.-J. *Inorg. Chem.* **1983**, *22*, 2953−2956.
(70) Wieghardt, K.; Kuppers, H.-J.; Weiss, J. *Inorg. Chem.* **1985**, *24*, 3067−3071.
(71) Kennepohl, P.; Solomon, E. I. *Inorg. Chem.* **2003**, *42*, 689−695.

Table 2. Total Intensity, Experimental Total Metal Character in Unoccupied Orbitals, DFT Calculated Covalency, and Covalency Based on VBCI Simulations for $K_4[FeCN)_6]$, $[Fe(tacn)_2]Cl_2$, $K_3[Fe(CN)_6]$, and $[Fe(tacn)_2]Cl_3$

compound	intensity	sum of the metal character in unoccupied orbitals (error)[a]	total unocc.	DFT (% metal character)					VBCI			
				Fe (t_{2g})	Fe (e_g)	Fe $\pi^*(t_{2g})$	Fe $\pi_b(t_{2g})$	Fe $\sigma^*(e_g)$	Fe (t_{2g})	Fe (e_g)	Fe $\pi_b(t_{2g})$	Fe $\pi^*(t_{2g})$
$K_4[Fe(CN)_6]$	36(4)	287(30) {72}	314	77	57	16	8	6		45		19
$[Fe(tacn)_2]Cl_2$	37(5)	295(40) {74}	322	93	72				93	72		
$K_3[Fe(CN)_6]$	43(5)	334(40) {67}	397	75	54	14	11	2	60	47	26	14
$[Fe(tacn)_2]Cl_3$	41(5)	326(40) {65}	345	92	64				93	63		

[a] Numbers given in the form A(B) {C}, where A is the sum of the metal character in unoccupied orbitals, (B) is the error on A, and {C} gives the hole-weighted average metal character (the sum of the % metal character in unoccupied orbitals/number of unoccupied orbitals).
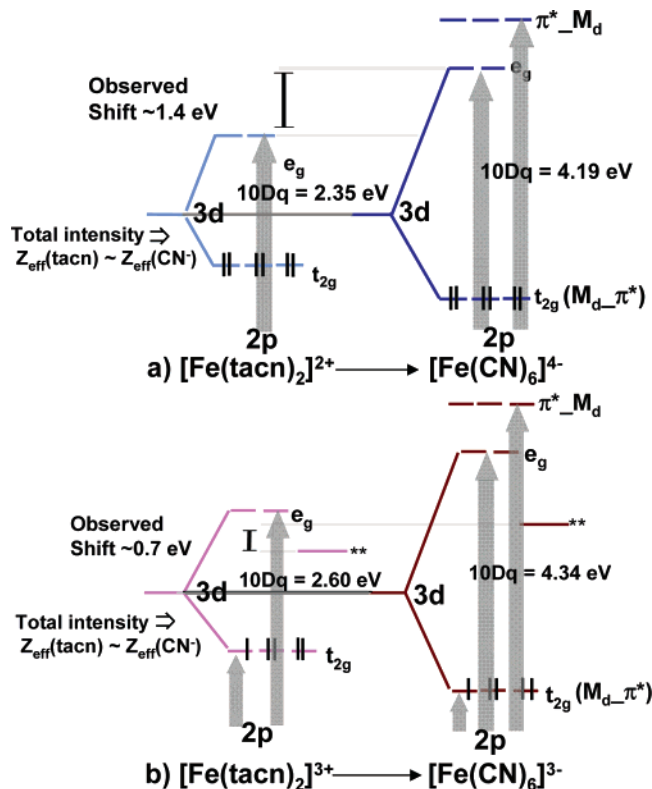

Figure 3. Schematic of the relative effects of Z_{eff} and 10Dq on the Fe L-edge energy shifts for (a) Fe(II) and (b) Fe(III) CN^- and tacn complexes. Gray arrows represent the orbitals to which transitions are observed; ** represents the energy-weighted average energy of the unoccupied d orbitals. Lines between the CN^- and tacn energy splittings are intended for reference.

This is the net effect of donation, which lowers Z_{eff}, and back-bonding, which increases it. The relative contributions of donation and back-bonding can be determined through an analysis of the spectral shape of the L-edge given below.

2. Effects of π-Back-Bonding on L-Edge Spectral Shape. To study the effects of π back-bonding on the L-edge multiplet structure, a set of systematic simulations were performed (Figure 4). The parameter space was simplified in two ways. First, no e_g mixing (i.e., σ bonding or σ back-bonding) was allowed, so any spectral change reflects the π back-donation. Second, the energy separation (Δ) between the d^N and $d^{N-1} L^-$ configurations was made numerically identical in the ground and excited states.[72] This requires that the wave function coefficients in the ground and excited states are identical. In this limit, no electronic relaxation occurs, so no intensity is redistributed due to satellite peaks (see section 3).[73,74] This enables identification of sys-
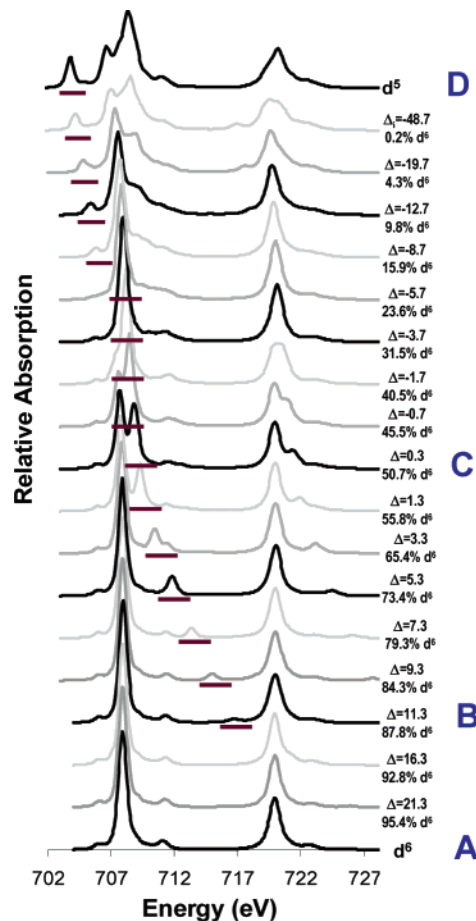
(72) Within the multiplet program, this is equivalent to setting the parameter EG2 = EF2 = X.

Figure 4. Set of systematic simulations for $|t_{2g}^6\rangle + |t_{2g}^5 L^-\rangle$, in which 10Dq = 3.5 eV and Δ was varied through the simulations. To simplify the calculations, relaxation was set to zero. The simulations clearly display the appearance of spectra with the secondary peak structure. The letters A−D indicate specific simulations referred to in the text.

tematic changes in L-edge spectra which are a consequence of ligand π^* effects. The relationship of Δ and the two configurations, d^6 and $d^5 L^-$, is illustrated in Figure 5.[45,71,73−76]

When π back-bonding is present in a system, there are two major sets of 2p → 3d transitions. There are transitions to the e_g set, which are also present in the absence of π back-bonding, and there are additional transitions to π^* orbitals. These two pathways are shown by the gray arrows in Figure 3a, right. A diagram representing the ground-state interaction of the metal

(73) Hu, Z.; Mazumdar, C.; Kaindl, G.; de Groot, F. M. F.; Warda, S. A.; Reinen, D. *Chem. Phys. Lett.* **1998**, *297*, 321−328.
(74) Hu, Z.; Kaindl, G.; Warda, S. A.; Reinen, D.; de Groot, F. M. F.; Muller, B. G. *Chem. Phys.* **1998**, *232*, 63−74.
(75) Kennepohl, P.; Solomon, E. I. *Inorg. Chem.* **2003**, *42*, 679−688.
(76) Kennepohl, P.; Solomon, E. I. *Inorg. Chem.* **2003**, *42*, 696−708.
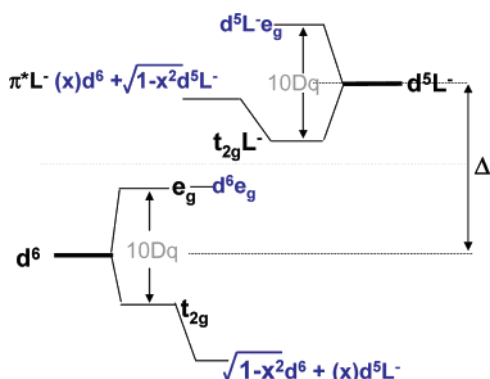
Figure 5. Diagram showing the d^6 and $d^5 L^-$ configurations separated by Δ and mixed by $T_{t_{2g}}$ in the ground state.

d^6 configuration and the ligand $d^5 L^-$ configuration is given in Figure 5. The two configurations are separated by Δ, and states of like symmetry can be mixed using the parameter T ($T_{t_{2g}}$ and T_{e_g} in O_h symmetry), which quantitates orbital overlap. Figure 5 shows that the lowest-energy metal-based orbitals of t_{2g} symmetry are occupied; thus, there can be no $2p \rightarrow 3d(t_{2g})$ transition. When t_{2g} mixing is "turned on" (i.e., $T_{t_{2g}} > 0$), these orbitals mix with the $CN^- \pi^*$ orbitals of t_{2g} symmetry. This mixes metal d character into the unoccupied ligand π^* orbitals.

Figure 4 shows how the simulated spectra change as Δ is systematically varied for a fixed 10Dq (3.5 eV) and mixing parameter T: 2 eV for the t_{2g} set ($T_{t_{2g}}$) and 0 eV for the e_g set (T_{e_g}).[73,74] The numerical values of T and Δ determine the coefficients in the expression $\Psi_{gs} = \alpha|d^N\rangle + \beta|d^{N-1} L^-\rangle$. When Δ is large and positive, the $|t_{2g}^5 L^-\rangle$ MLCT state is at a high energy above the $|t_{2g}^6\rangle$ state and no mixing between them occurs, resulting in a pure $|t_{2g}^6\rangle$ ground state (point A in Figure 4). In the reverse situation, where Δ is large and negative, a pure $|t_{2g}^5 L^-\rangle$ ground state results (point D in Figure 4). As Δ is systematically varied, the energy separation between the $|t_{2g}^6\rangle$ and $|t_{2g}^5 L^-\rangle$ configurations is reduced, and the metal d and ligand π^* orbitals of t_{2g} symmetry are allowed to mix. The spectral consequences of this are first noticeable at point B, where an additional peak (red underline in Figure 4) can be seen. As Δ is systematically reduced, the wave functions become more mixed and the π^* peak gains intensity and shifts closer in energy to the main e_g peak. As the e_g and π^* peaks become close in energy, the π^* peak derives intensity from the e_g peak, which is reduced in intensity. Eventually, Δ becomes negative, and the resulting spectrum has more $3d^5$ than $3d^6$ character.

Starting from the ground configuration, which includes π back-bonding $\alpha_1|t_{2g}^6 e_g^0\rangle + \beta_1|t_{2g}^5 e_g^0 L^-\rangle$, exciting an electron from the 2p orbital will produce three excited configurations:
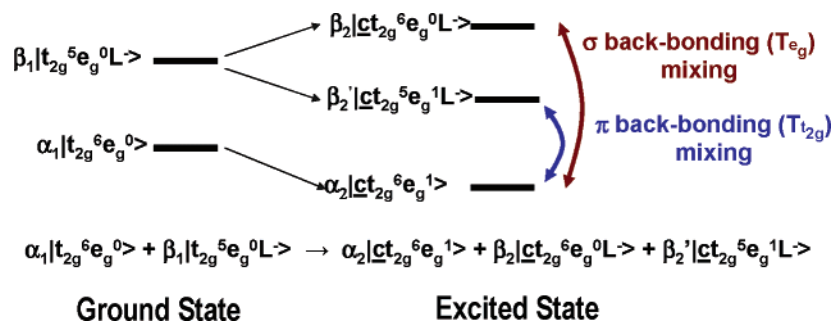
$\alpha_2|\underline{c}t_{2g}^6 e_g^1\rangle$, $\beta_2|\underline{c}t_{2g}^5 e_g^1 L^-\rangle$, and $\beta_2'|\underline{c}t_{2g}^6 e_g^0 L^-\rangle$ ($\underline{c}$ = 2p core hole). There are, in fact, two contributions to the new feature underlined in red in Figure 4. First, metal d mixing into the ligand π^* orbital provides a direct d contribution to the L-edge intensity, $\beta_2'|\underline{c}t_{2g}^6 e_g^0 L^-\rangle$. Second, there is also CI mixing in the excited state which involves $\beta_2|\underline{c}t_{2g}^5 e_g^1 L^-\rangle$ with $\alpha_2|\underline{c}t_{2g}^6 e_g^1\rangle$, as illustrated in blue in Figure 6. This excited-state mixing mechanism allows for the π^* feature, underlined in Figure 4, to "borrow" intensity from the main e_g feature, causing enhanced spectral changes due to π back-bonding. This mechanism for intensity borrowing also exists for Fe(III) through mixing the excited configurations $\beta_2|\underline{c}t_{2g}^4 e_g^1 L^-\rangle$ and $\alpha_2|\underline{c}t_{2g}^5 e_g^1\rangle$.

3. Effects of Electronic Relaxation. In the excited state, the $2p \rightarrow 3d$ X-ray absorption process creates a 2p core hole. This core hole lowers the energy of the d orbitals and changes their mixing with the ligand orbitals in the excited state. For a LMCT process, the Δ between the d^N and the $d^{N+1} \underline{L}$ configurations decreases upon electronic relaxation; for a MLCT process, Δ between the d^N and $d^{N-1} L^-$ configurations increases. To evaluate the effects of electronic relaxation, the simulations given in Figure 4 were extended to include a 2 eV change in Δ between the ground and the core hole excited states. Figure 7
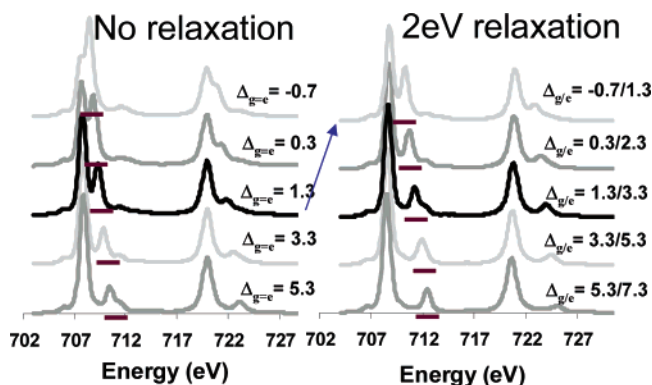

Figure 7. Comparison of a set of systematic simulations with no electronic relaxation and 2 eV electronic relaxation effects included.

compares a series of L-edge simulations with no electronic relaxation (left, Figure 7) and a series with a 2 eV change in Δ due to electronic relaxation (right, Figure 7). In the absence of electronic relaxation, we observe the "double-peaked" L_3-edge spectrum when $\Delta_{g/e} = 1.3$; in the series with electronic relaxation, the double-peaked spectrum is observed with $\Delta_g = -0.7$, $\Delta_e = 1.3$.[38] Thus, the Δ in the excited state is the dominating determinant of spectral shape.

4. Simulation of the Spectra of K₄[Fe(CN)₆] and K₃[Fe-(CN)₆]. a. K₄[Fe(CN)₆], t_{2g}^6. A superposition of the experi-

$\alpha_1|t_{2g}^6 e_g^0\rangle + \beta_1|t_{2g}^5 e_g^0 L^-\rangle \rightarrow \alpha_2|\underline{c}t_{2g}^6 e_g^1\rangle + \beta_2|\underline{c}t_{2g}^6 e_g^0 L^-\rangle + \beta_2'|\underline{c}t_{2g}^5 e_g^1 L^-\rangle$

Ground State   **Excited State**

Figure 6. Configurations involved in the ground and excited states, and the mechanisms by which they can mix.
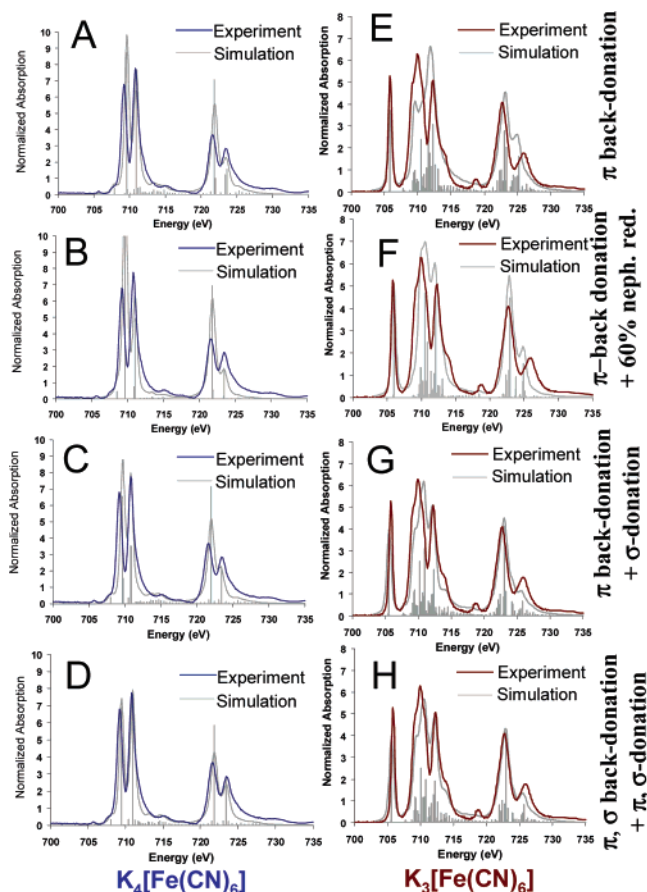
Figure 8. Simulations of the spectra of K₃[Fe(CN)₆] (A−D) and K₄[Fe-(CN)₆] (E−H). Simulations A and E include just the effects of π back-bonding; simulations B and F include the effects of π back-bonding and nephelauxetic reduction of electron repulsion; simulations C and G include π back-bonding and σ donation; and simulations D and H include π back-bonding, π donation, σ donation, and σ back-donation.

mental spectrum (blue) and a simulated spectrum (gray), which only includes the effects of back-bonding, is given in Figure 8A. For Fe(II), this simulation reproduces the shape of the experiment reasonably well, the two main features being similar to the experiment at both the L_2 and L_3 edges. σ donation has two contributions. The first is the reduction in electron repulsion known as the nephelauxetic effect, which is usually around 60% of the experimental free ion value.[77] The second is the LMCT mixing into the metal e_g set. In past multiplet simulations of this type,[41−43] it was not possible to include both LMCT and MLCT in one simulation. Here, the simulations can now explicitly include both.[77,78]

Figure 8B shows the results of a simulation which included the effects of back-bonding by charge transfer and the addition of a nephelauxetic reduction of 60%. The effect of nephelauxetic reduction on the spectral shape is very small; it acts to make the spectrum slightly sharper. Adding σ donation explicitly with LMCT has a similar effect, though it causes slight changes in the energy positions of the π^* and e_g peaks (Figure 8C). These observations indicate that π back-bonding provides the dominant effect on the Fe L-edge spectral shape of K₄[Fe(CN)₆]. The effect of systematically adding nephelauxetic reduction (Figure S6) and the effect of too much σ donation relative to π (Figure S5) are shown in the Supporting Information.

Finally, two additional effects were included in the final simulations of the L-edge spectra of K₄[Fe(CN)₆], π donation

and σ back-donation. The addition of π donation (from the filled π MO on the CN⁻ ligand) did not have a substantial effect on the spectral shape, since the t_{2g} orbitals are filled. σ back-donation (into the σ^* MO of the CN⁻ ligand) would not normally be thought to play a role in the bonding, because in low-spin Fe(II) complexes the e_g set of d orbitals in the ground state is empty. However, in an L-edge X-ray absorption process, the excited state has a $t_{2g}^6 e_g^1$ electron configuration, which has an e_g electron available to undergo σ back-bonding (Figure 6). When the effects of σ back-bonding are included in the simulation, the spectrum becomes broader and gives slightly better agreement with experiment (Figure 8D).

b. K₃[Fe(CN)₆], t_{2g}^5. For this low-spin Fe(III) complex, simulated spectra which included only back-bonding did not have the well-resolved double-peaked structure at ∼710 eV found in the experimental spectrum (Figure 8E). The addition of σ donation by a nephelauxetic reduction of 60%, and by also including σ donation by charge transfer, improved the agreement between the experimental spectrum and the simulated spectrum (Figure 8F,G); π donation had the spectral effect of changing the intensity of the t_{2g} feature. The addition of a small amount of σ back-bonding improved the fit slightly, though the effect was less pronounced than in the case of Fe(II). The parameters of the final spectral fits for the Fe(II) and Fe(III) hexacyanides are given in Table 3.

5. Effects of 3d Spin−Orbit Coupling on the Spectra of Low-Spin Fe(III). In the spectra of both K₃[Fe(CN)₆] and [Fe-(tacn)₂]Cl₂, there is a significant peak to lower energy of the main multiplet packet that has been assigned as the t_{2g} feature.[38,66] In the experimental data, this feature is present on the low-energy side of both the L_3 and the L_2 edges; however, in simulations at 0 K, the t_{2g} feature on the low-energy side of the L_2 edge is absent (Figure 9, $J = 1/2$, Γ_7 spectral simulation).

The ground t_{2g}^5 configuration gives the $^2T_2$ ground state. Spin−orbit coupling gives $\Gamma_6 \otimes \Gamma_5 = \Gamma_7 + \Gamma_8(E_2 + G)$, of which Γ_7 ($J = 1/2$) is lowest in energy (Figure 10).[80] The $2p^5 t_{2g}^6$ excited configuration gives a $^2T_1$ excited state. This spin−orbit couples to give $\Gamma_6 \otimes \Gamma_4 = \Gamma_6 + \Gamma_8(E_1 + G)$; the "$t_{2g}$ peak" at the L_3 edge is the Γ_8 and at the L_2 edge is Γ_6. An electric-dipole-allowed transition ($T_1 = \Gamma_4$) from a Γ_7 ground state is given by $\Gamma_7 \otimes \Gamma_4 = \Gamma_7 + \Gamma_8$. Thus, the transition to the Γ_6 L_2 edge feature is not allowed, and only the L_3 t_{2g} peak has intensity. Alternatively, starting from the higher energy Γ_8 spin−orbit component of the $^2T_2$ ground state, transitions to both the L_2 (Γ_6) and L_3 (Γ_8) pre-edges have intensity $\Gamma_6 + \Gamma_7 + 2\Gamma_8$. These differences are clear from the multiplet simulations given in Figure 9, where those for the $J = 3/2$ and $J = 1/2$ states are separated. The energy separating the two components of the ground state is given by $(3/2)\lambda$, or ∼422 cm⁻¹. Thus, there is no thermal population of the Γ_8 component of the ground state, and it cannot contribute intensity to the L_2 pre-edge feature. However, this energy separation is small, and in real systems

(77) Jorgenson, C. K. *Prog. Inorg. Chem.* **1962**, *4*, 73−124.
(78) Note that the calculated atomic Slater, Condon, and Shortley parameters are larger than the experiment ones by a factor of ∼1.25; consequently, these parameters are usually reduced to 80% of the calculated free ion values. The nephelauxetic effect refers to a reduction over the free ion value.
(79) EG2/EF2 is the average energy separation between d⁵ L⁻ and d⁶ configuration and EG3/EF3 between d⁵ L⁻ and d⁷ L in the ground and the final states, respectively.
(80) Figgis, B. N.; Hitchman, M. A. *Ligand Field Theory and Its Applications*; Wiley-VCH: New York, 2000.

Table 3. Parameters for Three Configuration Simulations of $K_3[Fe(CN)_6]$ and $K_4[Fe(CN)_6]$

compound	10Dq	configuration separations[79]				mixing parameters			
		EG2	EF2	EG3	EF3	$d^5 \underline{L}^--d^6 \, T_{eg}$	$d^5 \underline{L}^--d^6 \, T_{t2g}$	$d^7 \underline{L}--d^6 \, T_{eg}$	$d^7 \underline{L}--d^6 \, T_{t2g}$
Fe(II)a. $K_4[Fe(CN)_6]$	3.7	2.06	1.56	−2.00	0.00	0.0/0.0	1.9	1.3	0.0
Fe(II)b. $K_4[Fe(CN)_6]$	3.9	2.06	1.56	−2.00	0.00	0.0/1.0	1.6	1.9	0.0
Fe(III)a. $K_3[Fe(CN)_6]$	3.8	1.00	0.50	1.00	1.50	0.0/0.0	2.0	2.2	0.0
Fe(III)b. $K_3[Fe(CN)_6]$	4.0	1.00	0.50	1.00	1.50	0.0/0.9	2.0	2.1	0.6

minor deviations from O_h symmetry will mix these two states (Figure 10).[45,81] A simulation done in D_{4h} symmetry (i.e., the dynamic Jahn−Teller effect for a $^2T_2$ ground state), with a separation between d_{xy} and $d_{xz/yz}$ of ∼700 cm^{-1}, is given in Figure 9, where the t_{2g} peak is now present at the low-energy side of the L_2 edge. Parameters of the D_{4h} simulation are given in the Supporting Information (Table S3 and Figure S8).

6. DFT Calculations. Spin-unrestricted density functional calculations using the BP86 functional were performed on $[Fe(CN)_6]^{4-}$ and $[Fe(CN)_6]^{3-}$ in O_h symmetry for comparison with the results of the spectral simulations. A summary of the % covalency from the experimental intensities, the simulations, and these DFT calculations (Mulliken population analysis) is given in Table 2.

The DFT-optimized geometries of $[Fe(CN)_6]^{3-}$ and $[Fe(CN)_6]^{4-}$ differ slightly from the crystal structures. First, both the DFT Fe−C and C−N bond lengths are longer than the experimental values. Second, crystallography consistently shows $[Fe(CN)_6]^{4-}$ to have shorter Fe−C distances than $[Fe(CN)_6]^{3-}$, whereas the DFT results give similar distances. For Fe(III), experiment (DFT) gives Fe−C = 1.941 (1.960) Å, C−N = 1.15 (1.180) Å, and for Fe(II), Fe−C = 1.915 (1.964) Å, C−N = 1.164 (1.192) Å. The population analyses at both the experimental and optimized geometries were the same within error. Population

Figure 9. Comparison of the experimental data (red) to spectral simulations, $J = \frac{1}{2}$, Γ_7 (gray), $J = \frac{3}{2}$, Γ_8 (dark gray), and D_{4h} (blue). Arrows indicate the "t_{2g} feature", arising from the $2p^6 t_{2g}^5 \rightarrow 2p^5 t_{2g}^6$ transition.

Figure 10. Spin−orbit and low-symmetry (D_{4h}) effects on the $^2T_{2g}$ ground state of low-spin d^5 complexes. (Left) $^2T_{2g}$ spin−orbit splits in the octahedral double group to give Γ_7 and Γ_8 states ($J' = \frac{1}{2}$ and $J' = \frac{3}{2}$). These are then low-symmetry split in the D_4' double group. To the right, the $^2T_{2g}$ state is split by a tetragonally elongated distortion (Δ), giving $^2B_{2g}$ and ^2E_g states, which under spin−orbit coupling give Γ_7, Γ_6, and Γ_7 states; the two limits are correlated.

analyses at the experimental geometries are given in the Supporting Information. The energy splittings obtained from DFT were close to those obtained by Hummel et al.[29] and reproduce closely the experimental values of 10Dq.[15] The HOMOs of both $[Fe(CN)_6]^{4-}$ and $[Fe(CN)_6]^{3-}$ are the metal-based orbitals of t_{2g} symmetry. For Fe(II), these orbitals have contributions from both CN$^-$ π-acceptor (14%) and CN$^-$ π-donor (8%) orbitals; for Fe(III), the π-acceptor contribution decreases relative to that for Fe(II) to 12%, and the π-donor contribution increases to 11%. The CN$^-$ π-acceptor contributions to the t_{2g} set of "d" orbitals are reciprocated, with metal t_{2g} character mixed into the CN$^-$ π^* orbitals: 16% metal character for Fe(II) and 14% metal character for Fe(III). Thus, on the basis of calculations, CN$^-$ back-bonds slightly more to Fe(II) than to Fe(III) and acts as a strong π-donor to Fe(III). (Note that there is no net π donation in the Fe(II) complex, since the t_{2g} set of d orbitals are fully occupied.) The coefficients of the metal-based e_g orbitals are indicative of the amount of σ donation. For Fe(II), there is slightly more metal character in the e_g orbitals (57%) compared to that for Fe(III) (54%). The difference is mostly due to the differences in CN$^-$ σ-donor character, which is 36% in Fe(II) and 42% in Fe(III); however, there is also a small percentage of CN$^-$ σ^*-acceptor character. This contribution is 7% in Fe(II) and 2% in Fe(III) and results in some metal $d\sigma$−e_g character mixing into the CN$^-$ σ^* MO, which lies 1.7 eV above CN$^-$ π^* for Fe(II) and 3.0 eV above π^* for Fe(III). This interaction does not contribute to the bonding in the ground state but can affect the excited state of the L-edge X-ray absorption spectrum, as described in section 4.

This set of DFT calculations produce orbital coefficients for the Fe(II) and Fe(III) hexacyanides in the range that has been reported previously.[17,27,28,30,33] The total metal character in unoccupied orbitals is calculated with BP86 to be slightly lower than from the L-edge intensity (Table 2). For Fe(II), the experiment-to-calculated ratio of total d character is 287(31):314; for Fe(III), this ratio is 334(40):397.

The VBCI spectral simulations performed in section 4 can be interpreted in terms of differential orbital covalency.[38] When projected (see Table 2 and Figure 8 for details), the final simulation of $K_4[Fe(CN)_6]$ gives the e_g set as having 45(5)% metal character and the CN$^-$ π^* set as having 19(3)% metal character. The VBCI analysis of the experimental spectra gave an overall more covalent system than the DFT calculations (Table 2 and Figure 11, left), which gave the e_g set as having 57% metal character and the CN$^-$ π^* orbital as having 16% metal character. For Fe(III), the VBCI simulation of $K_3[Fe(CN)_6]$ gives 47(5)% metal character in the e_g set, 60(6)% metal character in the t_{2g} set, and 14(2)% metal character in the CN$^-$ π^* orbital set, indicating a 26% contribution of π donation. The DFT-calculated values are 54% for the e_g and 14% for the CN$^-$
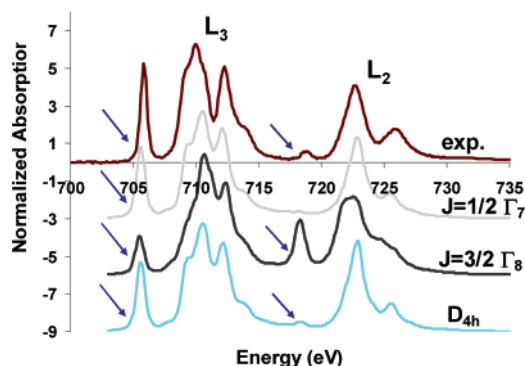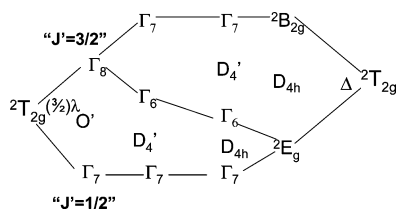
(81) deGroot, F. M. F.; Hu, Z. W.; Lopez, M. F.; Kaindl, G.; Guillot, F.; Tronc, M. *J. Chem. Phys.* **1994**, *101*, 6570−6576.

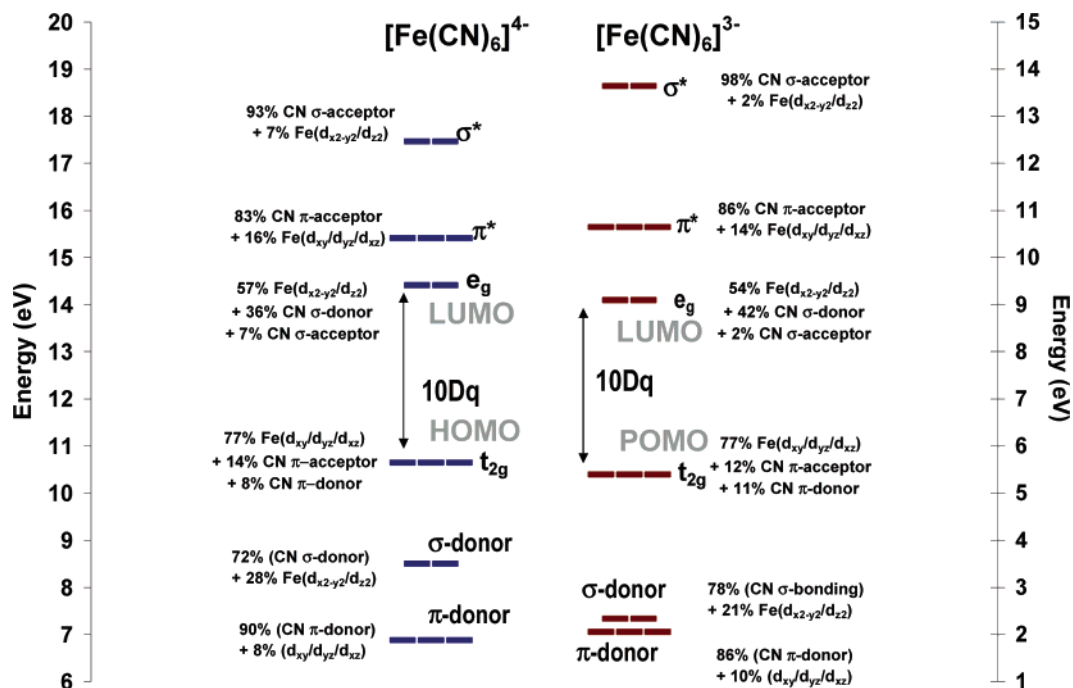**Figure 11.** Energy level diagram for $[Fe(CN)_6]^{4-}$ and $[Fe(CN)_6]^{3-}$. The orbital coefficients are given, offset to the left for Fe(II) and to the right for Fe(III). For $[Fe(CN)_6]^{3-}$, only the β-spin orbitals are given. The α-spin molecular orbitals are given in the Supporting Information. POMO stands for partially occupied molecular orbital, as the three-fold degenerate β t_{2g} levels in Fe(III) low-spin compounds contain two electrons.

π^* orbitals, with an 11% contribution from π donation. The VBCI simulations predict back-bonding to be more dominant in Fe(II) than in Fe(III). The experimental and theoretical values reflect the differences between Fe(II) and Fe(III) hexacyanides observed using other experimental techniques, predicting the back-bonding to be slightly greater in Fe(II) than in Fe(III) and σ donation being the same, within error, for both.[17,27,28,30,33]

Discussion

Many techniques have been applied to understand the nature of metal−ligand back-bonding, yet all are beset by complications when trying to separate the effects of σ donation from those of π back-donation.[7−12] The Fe L-edge is the consequence of a 2p $\rightarrow$ 3d transition. This transition is electric dipole allowed, so the intensity arises from metal d character in unfilled valence orbitals.[38] In systems with back-bonding, there are additional transitions to ligand-based π^* orbitals which can dramatically change the spectral shape and intensity of the L-edge. The dominance of the π^* back-bonding on the spectroscopic structure at the L-edge derives from the fact that π^* mixes the multiplet intensity associated with transitions to the metal e_g orbitals into the ligand-based π^* orbitals in the excited state. In Figure 12, the effects of back-bonding are systematically evaluated. Spectrum A is the L-edge multiplet structure with no back-bonding. Spectrum B has back-bonding included in the ground state, and spectrum C allows for back-bonding in both the ground and the excited states. On going from spectrum A to B, we see an additional, relatively weak shoulder to higher energy, indicated by the red arrow. This shoulder derives from the additional transition intensity to ligand-based π^* orbitals with metal d character from the occupied t_{2g}^6 configuration mixed into them through back-bonding. A much larger difference is observed on going from spectrum B to C, where an additional intense transition to the CN^- π^* is now present. Here, the wave function coefficients in the ground state are the same
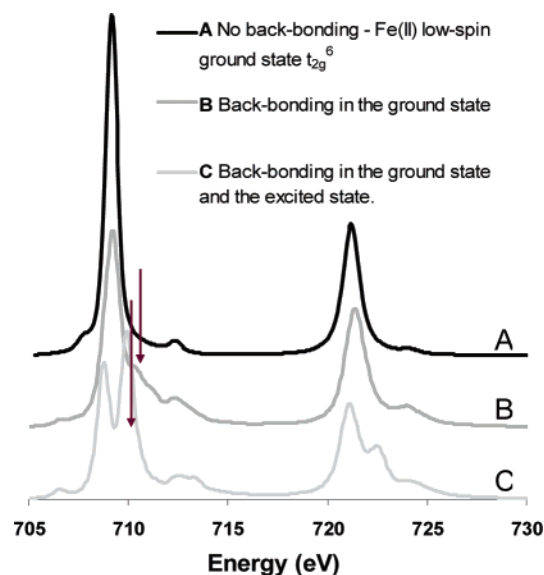

Figure 12. Effect of back-bonding on an L-edge: (A) no back-bonding (pure Fe(II) low-spin $(t_{2g})^6$ ground state); (B) π back-bonding in the ground state; and (C) back-bonding in the ground and excited states.

as in B; however, in the excited state, the back-bonding allows the π^* transition to "borrow" intensity from the intense metal-based e_g transitions (Figure 6, blue). This excited-state mixing is responsible for the distinct double-peaked feature of the iron hexacyanide L-edge spectra. Thus, the L-edge provides a sensitive and direct probe of back-bonding and allows it to be quantified. The analysis of the $K_4[Fe(CN)_6]$ L-edge (Figure 8G) gives the % metal character in the π^* orbital as 18(3)%. The VBCI analysis of the L-edge of $K_3[Fe(CN)_6]$ gives the π^* orbital as having 14(2)% metal character. These values are in the same range as those predicted by calculations reported both here and elsewhere.[16,17,27,29,30] They also agree well with the more qualitative results of other experimental techniques, including

X-ray crystallography,[82−84] absorption,[15] and IR spectroscopy.[20,21,23,26] We also note that there are other methods that could potentially quantify the amounts of back-bonding, including ligand K-edge XAS and XPS through shake-down satellites; however, these have not yet been developed sufficiently for this purpose.[11,12,85]

Finally, there is an important point to make about the relationship of the edge energy shift to the Z_{eff} and ligand field. The total intensity of the L-edge reflects the total metal d character in the unoccupied orbitals and probes the sum of net donation and back-donation. Thus, the total intensity directly probes the Z_{eff} of the metal center in the complex. Upon going from the tacn to cyanide ligand sets for both the Fe(II) and Fe-(III) complexes, very little total L-edge intensity change is observed. This indicates that the metal Z_{eff} does not significantly change between the tacn and cyanide compounds (i.e., for the cyanides the increase in σ donation is compensated by the presence of back-bonding). However, the ligand field does substantially increase upon going from a tacn to a cyanide donor set, by ~2 eV for both Fe(II) and Fe(III).[68−70] Since the L-edge shifts up in energy and Z_{eff} does not change, the shifts in L-edge energy to higher values must reflect the field strength of the CN^- ligand.

In summary, many different experimental techniques have been applied to probe the bonding in the ferri- and ferro-hexacyanides. Here, we have used these classic compounds to evaluate the sensitivity of Fe L-edge XAS as a probe of metal-to-ligand back-bonding. Back-bonding in $[Fe(CN)_6]^{3-}$ and $[Fe(CN)_6]^{4-}$ results in an additional intense Fe L-edge feature. The nature of this feature and the origin of its high intensity have been determined. Analysis of this feature, combined with the rest of the L-edge spectral shape, the edge energy shift, and total intensity, allows us to use Fe L-edge XAS to uncouple and quantify the effects of σ donation and π back-donation in metal complexes, thus demonstrating the application of Fe L-edge XAS as a direct probe of metal−ligand donation and, in particular, back-bonding.

Supporting Information Available: Complete ref 58; composition of BP86 MOs for Fe(III) α- and β-spins; comparison of the contributions calculated at both the crystal structure geometries and geometry optimized structures; schematic of the relationship between the different configurations; tabulation of the edge shifts between tacn and CN^- spectra; tabulation of the experimental metal−ligand distances, 10Dq values, and nephelauxetic parameters available for $[Fe(tacn)_2]^{2+/3+}$ and $[Fe(CN)_6]^{4-/3-}$; scatter plot of the available crystallographic data for $[Fe(CN)_6]^{4-}$ and $[Fe(CN)_6]^{3-}$; effect of simulating the spectra with only π back-donation and the systematic addition of nephelauxetic reduction; examination of the spectral effect of adding too much σ donation; effects of d−d spin−orbital coupling on the spectra of $[Fe(tacn)_2]Cl_3$; blow-up of the simulations given in Figure 8; input parameters used to generate the D_{4h} simulation given in Figure 9; expansion of Figure 10 including frontier molecular orbitals; and input files for the TT-multiplets program. This material is available free of charge via the Internet at http://pubs.acs.org.

JA061802I

(82) Popelov, V. A.; Zhdanov, G. S. *J. Chem. Phys. (U.S.S.R.)* **1947**, *21*, 879−881.
(83) Van Bever, A. K. *Recl. Trav. Chem.* **1938**, *57*, 1259−1261.
(84) These references are to the original crystallography on the molecules; the geometric parameters of modern structures are substantially more accurate. A scatter plot of the available structural data is given in Figure S4.
(85) Prins, R.; Biloen, P. *Chem. Phys. Lett.* **1975**, *30*, 340−434.